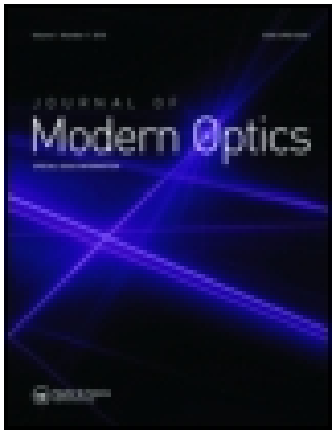

Journal of Modern Optics
Publication details, including instructions for authors and subscription information:
http://www.tandfonline.com/loi/tmop20

An ultra-compact tunable Bragg reflector based on edge propagating plasmons in graphene nanoribbon

Zhen-Rong Huang[a], Ling-Ling Wang[a], Meng-Dong He[b], Hong-Ju Li[a], Bin Sun[a], Jian-Qiang Liu[c] & Xiang Zhai[a]

[a] School of Physics and Microelectronic and Key Lab for Micro-Nano Physics and Technology of Hunan Province, Hunan University, Changsha, China.

[b] Institute of Mathematics and Physics, Central South University of Forestry and Technology, Changsha, P.R. China.

[c] School of Science, Jiujiang University, Jiujiang, China.

Published online: 08 Dec 2014.

To cite this article: Zhen-Rong Huang, Ling-Ling Wang, Meng-Dong He, Hong-Ju Li, Bin Sun, Jian-Qiang Liu & Xiang Zhai (2014): An ultra-compact tunable Bragg reflector based on edge propagating plasmons in graphene nanoribbon, Journal of Modern Optics, DOI: 10.1080/09500340.2014.989926

To link to this article: http://dx.doi.org/10.1080/09500340.2014.989926

Journal of Modern Optics, 2014
http://dx.doi.org/10.1080/09500340.2014.989926

Taylor & Francis
Taylor & Francis Group

An ultra-compact tunable Bragg reflector based on edge propagating plasmons in graphene nanoribbon

Zhen-Rong Huang[a], Ling-Ling Wang[a]*, Meng-Dong He[b], Hong-Ju Li[a], Bin Sun[a], Jian-Qiang Liu[c] and Xiang Zhai[a]

[a]*School of Physics and Microelectronic and Key Lab for Micro-Nano Physics and Technology of Hunan Province, Hunan University, Changsha, China;* [b]*Institute of Mathematics and Physics, Central South University of Forestry and Technology, Changsha, P.R. China;* [c]*School of Science, Jiujiang University, Jiujiang, China*

(*Received 22 July 2014; accepted 17 November 2014*)

A mid-infrared planar Bragg reflector, which is based on the fundamental edge plasmonic mode in the nanoribbons is proposed and numerically demonstrated in this paper. The simulation results calculated with the three-dimensional (3D) finite element method reveal that it shows superb wide-band filtering characteristics in the mid-infrared frequencies, and the bandwidth of stopband in the reflector can be dynamically modulated by varying the chemical potentials of corresponding nanoribbon waveguides. In addition, its band properties on the ribbon width are also analyzed. This kind of Bragg reflector exhibits extreme compactness of lateral scales and wonderful light confinement in both the longitudinal and the lateral directions, which is expected to have significant applications in constructing 3D highly integrated optical networks for signal processing.

Keywords: surface plasmon polaritons; Bragg reflector; graphene

1. Introduction

Surface plasmon polaritons (SPPs) [1], which are coupled electromagnetic modes of exciting photons and surface electrons in conductors or semiconductors, have been considered as the most potential way for the realization of highly integrated optical systems for their ability of manipulating and channeling light in subwavelength limit. Graphene as an atomically thin material has recently been manifested to be capable of supporting both TE and TM polarized SPP mode [2]. Compared with noble metals, the graphene presents unique plasmonic properties, such as tunability [3–5], extreme confinement [6], long lifetimes and low loss [7]. These merits have spurred tremendous interests on this one-atom thin material [8], from which various applications, such as modulators [9,10], splitters [11] and switches [12] are rapidly emerging. Among those charming advantages, the most attractive one is its dielectric function can be rapidly modulated via changing its chemical potential by utilizing an external electric field or biased gate voltage [13]. This enables one to tame electromagnetic into desired shapes, which provides a viable path to devise novel planar photonic elements, such as waveguides [2], Luneburg lenses [14], and filters [15] on this single atom platform. With regard to achieving the ultimate goal of realizing highly integrated optical circuits, the graphene nanoribbon is also demonstrated to possess great potential in constructing ultra-compact photonic elements [16]. This is mainly due to its supported unique edge plasmonic mode [17], which exhibits many intriguing characteristics in both information transferring and exchange at nanoscales [18].

The Bragg reflector is one kind of crucial elements in the photonics, because of its significant applications in several optoelectronic devices, such as filters, modulators, light-emitting diodes, and resonant-cavity photodetectors [19,20]. For the past decades, investigations on the plasmonic Bragg reflectors are mainly based on insulator-metal-insulator or metal-insulator-metal waveguides [21,22], each of them have their own merits and demerits. Nevertheless, both of these two kinds of Bragg reflectors are hardly tunable once the geometry of the structure is fixed, due to the fact that optical properties in metals are not easily to be modified. Graphene as a newly risen plasmonic material seems to provide a solution to this problem. Recently, the graphene-based Bragg reflector has been designed [23], which makes use of the high refractive indices contrast between the monolayer graphene and the graphene with dielectric substrate. It indeed presents advantageous tunability compared with noble metal based ones. However, from the view point of constructing three-dimensional (3D) integrated photonic networks, this kind of Bragg reflector

*Corresponding author. Email: llwang@hnu.edu.cn

may still face difficulties because of its infinite lateral scales. In fact, to the best of our knowledge, most of the previous studies about the planar plasmonic Bragg reflectors are concerned only in the two dimensions. A real 3D compact Bragg reflector, which can be incorporated into 3D highly integrated optical networks, still remains challenging and is urgently needed.

In this work, by taking advantage of the charming wave guiding performance of edge plasmonics in the nanoribbons, we demonstrate that a real compact 3D plasmonic Bragg reflector can be realized on this single atom platform. In addition, the real-time modulation of the reflector is achieved by dynamically tuning the chemical potentials in the respective nanoribbons. Furthermore, the influence of the ribbon width on its band characteristics is also analyzed. This kind of Bragg reflector exhibits wide band gap in the mid-infrared frequencies, and it is compact in size at both lateral scales, which is envisioned to play pivotal role in constructing highly integrated SPP based devices, such as distributed Bragg SPP emitter, filters, modulators, and other compact broad bandgap nanophotonic elements in ultra-compact optical systems.

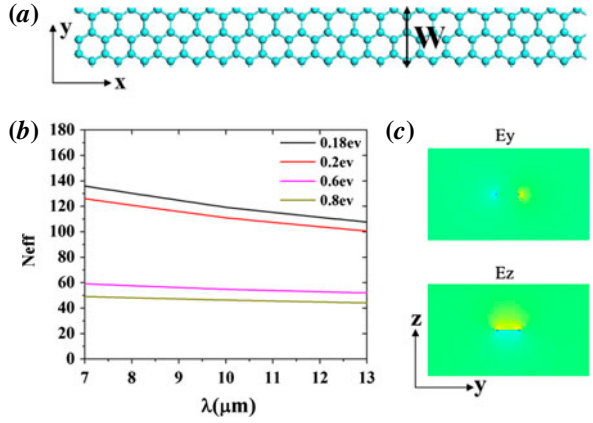

Figure 1. (*a*) Schematic diagram of the graphene nanoribbon waveguide with width W. (*b*) Dependence of the effective refractive index (N_{eff}) on the incident wavelength with various chemical potential (μ_c) in graphene. (*c*) The electric fields distribution (cross section) of the SPP mode in the nanoribbon with $\lambda = 10\,\mu\text{m}$ and $\mu_c = 0.6\,\text{ev}$. (The colour version of this figure is included in the online version of the journal.)

2. Results and discussion

The propagation characteristics of a freestanding graphene nanoribbon waveguide are studied firstly. As is shown in Figure 1(*a*), the graphene nanoribbon with a narrow width of W is modeled as an ultra-thin film with a thickness of Δ. The surface conductivity σ of the graphene is governed by Kubo formula [2,24], which relates to the radian frequency ω, temperature T, momentum relaxation time τ, and chemical potential μ_c. In this study, the light wavelength in free space is chosen to be in the mid-infrared range which is around $10\,\mu\text{m}$ ($\hbar\omega = 0.124\,\text{ev}$), and the considered minimum value of chemical potential μ_c is 0.18 ev. Thus, the conductivity contribution of the interband transition is neglected, because the chemical potential is always above half of the photo energy of incident light. Under this condition, the surface conductivity of grahene is reduced to a semiclassical Drude model at room temperature [25] ($\sigma(\omega) = i(e^2\mu_c/\pi\hbar^2)/(\omega + i\tau^{-1})$), where μ_c represents the absolute value of the chemical potential, and the carrier relaxation time $\tau = \mu\mu_c/(\text{ev}_f^2)$ relates to the carrier mobility μ and Fermi velocity $v_f = 10^6\,\text{m/s}$ in graphene. Here, μ is set to be $10,000\,\text{cm}^2/\text{V/s}$. The equivalent permittivity of graphene is given by [2,25] $\varepsilon_g = 1 + i\sigma\eta_0/(k_0\Delta)$ where η_0 ($\approx 377\Omega$) is the impedance of air and $k_0 = 2\pi/\lambda$ is the free-space wavenumber. The Δ is set to be 0.5 nm in this simulation, although other extreme values will lead to similar results. All calculations have been implemented using the commercial finite element method software COMSOL Multiphysics.

Figure 1(*a*) shows the schematic diagram of a graphene nanoribbon with a narrow width W. In terms of the graphene nanoribbon, it is well known that it supports two types of SP modes: one is the waveguide type, with the EM field concentrated at the whole area of the ribbon, and the other is the edge modes that the EM field is localized on the rims of the ribbons. They separated with each other by a wave-vector gap. However, when the width W is only dozens of nanometers, the nanoribbon waveguide only supports fundamental edge modes in the mid-infrared frequencies. Note that the microscopic details at the edges of the ribbons are not taken into consideration in the present study, which are similar to the treatment in some previous works [15–17,26]. The guided SPP mode, which takes the form $\vec{E}(\vec{r},t) = \vec{E}(y,z)\exp(iqk_0x)\exp(-i\omega t)$ (q is the modal wave vector) is excited by a discrete port that is placed in front of the graphene ribbon.

As shown in Figure 1(*b*), two representative groups of chemical potentials(μ_c) were selected, which consists of two large values (0.6 and 0.8 ev) and two small ones (0.18 and 0.2 ev), to analyze their influence on the effective refractive indices (N_{eff}) of SPPs supported in the nanoribbon waveguides. From Figure 1(*b*), one can clearly notice that the N_{eff} exhibits greater sensitivity to the changes for smaller chemical potentials than that for larger ones. When μ_c is 0.2 ev, a decrease of 0.02 ev in chemical potential would improve the N_{eff} by an average of 10. However, when μ_c is 0.8 ev, the N_{eff} only grow by 10.2 in average as the chemical potential drops from 0.8 to 0.6 ev. As is know that the chemical potentials in nanoribbon rest with its applied gate voltage or doping level, this feature indicates that a very tiny biased voltage or doping applied on the nanoribbon will induce a large variation of it's refractive index while μ_c is small. On the other hand, as refractive index

of the nanoribbon is determined by its chemical potentials based on the above discussion, the refractive index contrast of SPPs, therefore, can be directly generated by tuning the chemical potentials. As is displayed in Figure 1(*b*), a N_{eff} difference of 68.3 is obtained when $\mu_c = 0.2$ and 0.6 ev at wavelength of 7 μm. And this value increases to 88.2 when μ_c equals to 0.18 and 0.8 ev. Such feature provides us favorable condition to devise the tunable Bragg reflector on this single atom platform. Here, the ribbon width W is assumed to be 10 nm for the calculation. From Figure 1(*c*), one sees clearly that the symmetric fundamental edge mode with strong lateral confinement is supported in the ribbon region.

Figure 2 schematically illustrates the proposed Bragg reflector, which is constructed by periodically stacking graphene nanoribbon waveguides with patterned chemical potentials. The red-filled areas designate the ribbons (R_A) with large chemical potentials ($\mu_{c,A}$), and the navy blue filled ones correspond to the ribbons (R_B) with small chemical potentials ($\mu_{c,B}$). The length of R_A and R_B are labeled as L_A and L_B in Figure 2, respectively. The ribbon width is also set to be $W = 10$ nm. The $\mu_{c,A}$ is consistent with small refractive index and the $\mu_{c,B}$ corresponds to the large one. In terms of investigating the transmission property, the incident signal is injected from the port P_{in} with power A_1, and out of port P_{out} with power A_2, therefore the transmission is defined as $T = A_2/A_1$. It is well known that the nanoribbon can not only be an actual graphene strip, but also be virtually created on a monolayer graphene [17]. Consequently, as to realizing such a Bragg reflector experimentally, it can either be constructed on a real graphene strip, which may be cut out from a graphene sheet [27], or be virtually drawn on a single flake of graphene [2]. The second way may be achieved using different bias voltages to different regions in graphene to make the ribbon regions (red and navy blue filled areas in Figure 2) behave as metal to support SPPs, and at other areas, the graphene behaves as dielectric that cannot support them. The inhomogeneous patterned chemical potentials can be realized by adjusting the value and locations of applied bias voltages. We note that the calculations in this work are implemented for a free-standing graphene with no substrate. However, the concepts and effects introduced here will still be the same for graphene sheet standing on a substrate.

Based on Bragg condition $L_A N_{eff,A} + L_B N_{eff,B} = \lambda_b/2$ where λ_b is the Bragg wavelength, we can obtain a Bragg reflector operating around the middle infrared wavelength $\lambda_b = 10$ μm by suitably choosing the lengths or refractive index of the corresponding ribbons. Here, the length of R_A and R_B are fixed at $L_A = 20$ nm and $L_B = 35$ nm, respectively. Calculated with the mode solver in Comsol Multiphysics, we can obtain $N_{eff,A}$~46.38 at $\lambda = 10$ μm, which corresponds to $\mu_{c,A} = 0.8$ ev. To meet the Bragg condition, the $N_{eff,B}$ is choosen to be 116.4, which is related to $\mu_{c,B} = 0.184$ ev. The other $\mu_{c,A}$ and $\mu_{c,B}$ can be obtained by a similar way. Based on the above discussion, the simulated transmission spectra with different combination of $\mu_{c,A}s$ and $\mu_{c,B}s$ are obtained and shown in Figure 3. One can indeed see from the spectra that multiple wide bandgaps appear for the considered mid-infrared range. And different group of $\mu_{c,A}$ and $\mu_{c,B}$ results in different bandwidth of the stopband in the spectra. For example, in case of $\mu_{c,A} = 0.6$ ev and $\mu_{c,B} = 0.196$ ev (blue line in Figure 3), a bandwidth of 2.31 μm with near-zero transmission occurs around the central wavelength of 10 μm, which exhibits excellent wide band gap filtering characteristics. However, the bandwidth further increases to 2.77 μm when the difference between $\mu_{c,A}$ and $\mu_{c,B}$ gets enlarged, as is shown from the black line in Figure 3. This feature can be well understood by the fact that the refractive index contrast increases with the increase in the chemical potential difference, as is demonstrated in Figure 1(*b*). Therefore, when the chemical potential difference is reduced (i.e. $\mu_{c,A} = 0.4$ ev and $\mu_{c,B} = 0.224$ ev), the transmittance of the stopband is

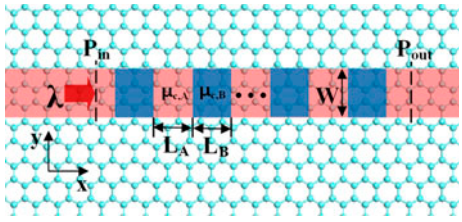

Figure 2. Schematic diagram of the Bragg reflector consisting of alternately stacked graphene nanoribbon waveguides (blue and red area in the picture) which is constructed on a single flake of graphene. The SPPs are only supported at the ribbon region and at other areas the graphene behave as dielectric. Here, L_A and L_B denote the length of the nanoribbon waveguide with chemical potential of $\mu_{c,A}$ and $\mu_{c,B}$, respectively. The width of the ribbon is denoted as W. The incident signal is injected through port P_{in} into the waveguide. (The colour version of this figure is included in the online version of the journal.)

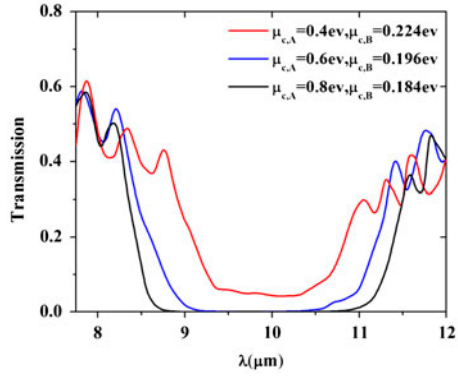

Figure 3. Transmission of the Bragg reflector consisting of eight periods with different chemical potential distributions. The width of the nanoribbon waveguide is $W = 10$ nm. (The colour version of this figure is included in the online version of the journal.)

correspondingly shortened to be 1.42 μm, as is shown from the red line in Figure 3, and the transmission in the stopband is lifted up at the same time. Through the above analysis, it can be concluded that by utilizing such scheme, one can modulate expediently the bandwidth of the reflector for a fixed central wavelength in the infrared range. Such function can be envisioned with promising potential for applications in future active integrated optical systems.

According to the transmission spectra shown in Figure 3, we also simulated the intensity distribution ($|E|^2$) of incident wave propagating through the structure at $\lambda = 8\,\mu$m and $\lambda = 10\,\mu$m, as shown in Figure 4, which are outside and inside the bandgap, respectively. From the top view of the distribution shown in Figure 4(*a*) and (*c*), where the monitor is placed 2 nm above the structure, one can indeed notice that the EM filed is tightly localized at the ribbon region in both the lateral dimensions. Simultaneously, strong light confinement also occurs for the structure in the longitudinal directions, as is shown in Figure 4(*b*) and (*d*) where the monitor is placed in the middle of the reflector. Taking the two noticeable facets of compactness and strong light confinement into considerations, our proposed Bragg reflector is very suitable for use in the 3D highly compact optical circuits, which shows charming properties compared with the previous proposed two-dimensional Bragg reflectors [21,23]. From Figure 4(*a*) and (*b*), one sees obviously from the intensity profile that when the Bragg condition is not satisfied, the incident light transmits efficiently through the ribbon. However, as shown in Figure 4(*c*) and (*d*), when the incident wavelength is inside the bandgap region, the plasmonic waves are thoroughly reflected by the reflector and cannot pass it.

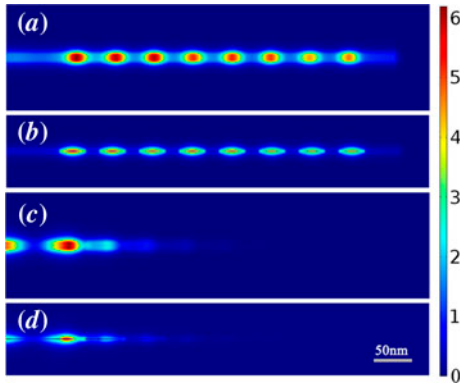

Figure 4. illustrate the intensity ($|E|^2$) distribution in the Bragg reflector as the incident light is outside [(*a*) and (*b*)] and inside [(*c*) and (*d*)] the bandgap with wavelength of $\lambda = 8\,\mu$m and 10 μm, respectively. Note that (*a*) and (*c*) demonstrate the top view (*x*-*y* plane), and (*b*) and (*d*) correspond to the side view (*x*-*z* plane) of the field intensity profile. The monitor in (*a*) and (*c*) is placed 2 nm above the structure and in (*b*) and (*d*), it's placed in the middle of the reflector. The chemical potentials in the reflector are set to be $\mu_{c,A} = 0.8$ ev and $\mu_{c,B} = 0.184$ ev respectively. (The colour version of this figure is included in the online version of the journal.)

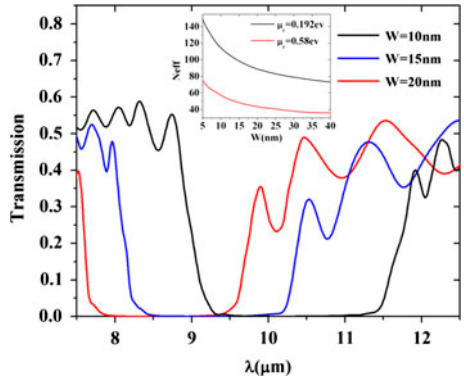

Figure 5. Transmission spectra of the Bragg reflector at different width (W) of the nanoribbon waveguide. The chemical potentials of the nanoribbon waveguides are set to be $\mu_{c,A} = 0.58$ ev and $\mu_{c,B} = 0.192$ ev, respectively. The inset depicts the dependence of the refractive index on the width of the ribbon. (The colour version of this figure is included in the online version of the journal.)

Despite the fact that the band characteristics of the Bragg reflector can be modulated by varying the chemical potentials, we also find that it's strongly dependent on the width of the nanoribbons. The dependence of the refractive indices on the width (W) of the nanoribbons is illustrated in the inset in Figure 5. From the diagram, one can clearly notice that the refractive indices will increase when ribbon width decrease, which is in consistent with the trend in Ref. [16]. However, the refractive indices of small chemical potential ($\mu_c = 0.192$ ev) increase at a faster rate than that of the large one ($\mu_c = 0.58$ ev). This will lead to the decrease in refractive index contrast as the ribbon width grows. For example, when $W = 10$ nm, the refractive index difference is 57.3. However, this value reduces to 45.4 when the W increases to 20 nm. The impact of these phenomena on the band property will be shown latter. As illustrated in Figure 5, we present the simulated transmission spectra of the reflector with various ribbon width. Two distinguished features can be drawn from the spectra. Firstly, the central wavelength of the Bragg reflector tends to blue-shift when the ribbon width increases. This can be understood according to the Bragg condition that the central wavelength reduces as the dwindling of optical length of the lattice constant $[L_A N_{eff,A} + L_B N_{eff,B}]$ lead by the decrease of refractive indices in the guide region. Secondly, the bandgap of the reflector shrinks accompanied with the reduction in central wavelength when W grows. According to the discussion about the inset in Figure 5, such rule can be well explained by the fact that the contrast of two nanoribbons in effective refractive indices will reduce when W increases. The above analysis indicates that the way of modulating the ribbon width indeed provides us new degree of freedom to manipulate the band characteristics.

3. Summary

In conclusion, a kind of tunable planar plasmonic Bragg reflector has been proposed and numerically investigated in this work based on the fundamental edge propagating plasmonics in the nanoribbon waveguide. The bandwidth of the stopband in the reflector can be dynamically modulated by tuning the chemical potentials in the respective nanoribbons. In addition, the dependence of the band characteristics on the ribbon width are also analyzed. Due to the compactness and strong light confinement of the reflector in both the lateral scales, it's expected to play significant role in building 3D ultra-compact SPP-based devices, such as filters, modulators, and other broad bandgap photonic elements for use in highly integrated optical circuits.

Funding

This work was supported by the National Natural Science Foundation of China [grant number 11074069], [grant number 11174372], [grant number 11264021], [grant number 61176116]; the Specialized Research Fund for the Doctoral Program of Higher Education of China [grant number 20120161130003].

References

[1] Barnes, W.L.; Dereux, A.; Ebbesen, T.W. *Nature* **2003,** *124,* 824–830.
[2] Vakil, A.; Engheta, N. *Science* **2011,** *332,* 1291–1294.
[3] Li, Z.Q.; Henriksen, E.A.; Jiang, Z.; Hao, Z.; Martin, M.C.; Kim, P.; Stormer, H.L.; Basov, D.H. *Nat. Phys.* **2008,** *4,* 532–535.
[4] Efetov, D.K.; Kim, P. *Phys. Rev. Lett.* **2010,** *105,* 256805-1–256805-4.
[5] Yan, H.; Li, X.; Chandra, B.; Tulevski, G.; Wu, Y.; Freitag, M.; Zhu, W.; Avouris, P.; Xia, F. *Nat. Nanotechnol.* **2012,** *7,* 330–334.
[6] Koppens, F.H.L.; Chang, D.E.; García de Abajo, F. J. *Nano Lett.* **2011,** *11,* 3370–3377.
[7] Gan, C.H.; Chu, H.S.; Li, E.P. *Phys. Rev. B* **2012,** *85,* 125431-1–125431-9.
[8] Ju, L.; Geng, B.; Horng, J.; Girit, C.; Martin, M.; Hao, Z.; Bechtel, H.A.; Liang, X.; Zettl, A.; Shen, Y.R.; Wang, F. *Nat. Nanotechnol.* **2011,** *6,* 630–634.
[9] Liu, M.; Yin, X.; Ulin-Avila, E.; Geng, B.; Zentgraf, T.; Ju, L.; Wang, F.; Zhang, X. *Nature* **2011,** *474,* 64–67.
[10] Lee, C.C.; Suzuki, S.; Xie, W.; Schibli, T.R. *Opt. Express* **2012,** *20,* 5264–5269.
[11] Zhu, X.; Yan, W.; Asger Mortensen, N.; Xiao, S. *Opt. Express* **2013,** *21,* 3486–3491.
[12] Chu, H.S.; Gan, C.H. *Appl. Phys. Lett.* **2013,** *102,* 231107-1–231107-3.
[13] Grigorenko, A.N.; Polini, M.; Novoselov, K.S. *Nat. Photonics* **2012,** *6,* 749–758.
[14] Vakil, A.; Engheta, N. *Phys. Rev. B* **2012,** *85,* 075434-1–075434-4.
[15] Li, H.J.; Wang, L.L.; Liu, J.Q.; Huang, Z.R.; Sun, B.; Zhai, X. *Appl. Phys. Lett.* **2013,** *103,* 211104-1–211104-4.
[16] He, S.; Zhang, X.; He, Y. *Opt. Express* **2013,** *21,* 30664–30673.
[17] Nikitin, A.Y.; Guinea, F.; García-Vidal, F.J.; Martín-Moreno, L. *Phys. Rev. B* **2011,** *84,* 161407-1–161407-4.
[18] Christensen, J.; Manjavacas, A.; Thongrattanasiri, S.; Koppens, F.H.L. Javier García de Abajo, F. *ACS Nano* **2012,** *6,* 431–440.
[19] Zhao, D.; Chan, K.T.; Liu, Y.; Zhang, L.; Bennion, I. *IEEE Photon. Technol. Lett.* **2001,** *13,* 191–193.
[20] Rattier, M.; Benisty, H.; Stanley, R.P.; Carlin, J.-F.; Houdré, R.; Oesterle, U.; Smith, C.; Weisbuch, C.; Krauss, T. *IEEE J. Sel. Top. Quantum. Electron.* **2002,** *8,* 238–247.
[21] Hosseini, A.; Massoud, Y. *Opt. Express* **2006,** *14,* 11318–11323.
[22] Liu, J.-Q.; Wang, L.-L.; He, M.-D.; Huang, W.-Q.; Wang, D.; Zou, B.S.; Wen, S. *Opt. Express* **2008,** *16,* 4888–4894.
[23] Tao, J.; Yu, X.; Hu, B.; Dubrovkin, A.; Wang, Q.J. *Opt. Lett.* **2014,** *39,* 271–274.
[24] Chen, P.Y.; Alù, A. *ACS Nano* **2011,** *5,* 5855–5863.
[25] Wang, B.; Zhang, X.; Yuan, X.; Teng, J. *Appl. Phys. Lett.* **2012,** *100,* 131111-1–131111-4.
[26] Shi, X.; Han, D.; Dai, Y.; Yu, Z.; Sun, Y.; Chen, H.; Liu, X.; Zi, J. *Opt. Express* **2013,** *21,* 28438–28443.
[27] Ci, L.; Xu, Z.; Wang, L.; Gao, W.; Ding, F.; Kelly, K.F.; Yakobson, B.I.; Ajayan, P.M. *Nano Research* **2008,** *1,* 116–122.